High-pressure structural study of α-Mn: Experiments and calculations

Logan K. Magad-Weiss,[1] Adebayo A. Adeleke,[2] Eran Greenberg,[3] Vitali B. Prakapenka,[3] Yansun Yao,[2,*] and Elissaios Stavrou[1,†]

[1]*Physical and Life Sciences Directorate, Lawrence Livermore National Laboratory, Livermore, California 94550, USA*
[2]*Department of Physics and Engineering Physics, University of Saskatchewan, Saskatoon Saskatchewan, S7N 5E2, Canada*
[3]*Center for Advanced Radiation Sources, University of Chicago, Chicago, Illinois 60637, USA*

(Received 3 October 2020; revised 12 December 2020; accepted 16 December 2020; published 7 January 2021)

Manganese, in the α-Mn structure, has been studied using synchrotron powder x-ray diffraction in a diamond anvil cell up to 220 GPa at room temperature combined with density functional calculations. The experiment reveals an extended pressure stability of the α-Mn phase up to the highest pressure of this study, in contrast to previous experimental and theoretical studies. On the other hand, calculations reveal that the previously predicted hcp Mn phase becomes lower in enthalpy than the α-Mn phase above 160 GPa. The apparent discrepancy is explained due to a substantial electron transfer between Mn ions, which stabilizes the α-Mn phase through the formation of ionic bonding between monatomic ions under pressure.

DOI: 10.1103/PhysRevB.103.014101

I. INTRODUCTION

At ambient conditions manganese crystalizes in, unparalleled among the elements, the complex α-Mn structure [space group I-43m (217), $Z = 58$]. It was proposed [1] that the complexity (with a very large number of atoms in the cubic unit cell) of this structure originates from a combination of the presence of three electronic levels with comparable stability and magnetic ordering, resulting in different atomic sizes. Thus, Mn atoms with different atomic sizes are accommodated in different crystallographic sites; that is, Mn atoms behave as if they are different atoms with different sizes [1,2]. Indeed, the α-Mn phase is analogous to the χ phase in binary or ternary intermetallic systems [2].

One would expect that under pressure the suppression of the magnetic moments [3] will result in a pressure-induced phase transition towards a much simpler crystal structure with equal atomic size. Previous experimental x-ray diffraction (XRD) studies [2,4] reported a somewhat surprising stability of the α-Mn phase up to at least 150 GPa. At higher pressure, a phase transition was reported by Fujihisa and Takemura [2] based on the appearance of a new low-intensity Bragg peak above 165 GPa that coexisted with the main Bragg peak of the α-Mn phase up to 190 GPa. After considering three simple metallic structures (bcc, fcc, and hcp), a bcc structure was suggested as the high-pressure phase based on the lower volume collapse during the transition of the α-Mn to the bcc phase rather than the other two possible phase transitions. A follow-up first-principles theoretical study challenged this conclusion and predicted that the hcp phase has lower enthalpy than both the bcc and fcc phases in the 0–200-GPa pressure range and thus should be the high-pressure (HP) phase above 165 GPa [3]. However, the α-Mn phase was not included in the theoretical study, and therefore, the relative stability of the hcp over the α-Mn phase remains an open question.

To date, the crystal structure of the HP phase of Mn remains controversial: experimentally, the quality of the previous XRD study does not allow definitive indexing of the HP phase, and theoretically, the relative stability of the α-Mn and hcp phases was not examined. In order to address these issues, we have carried out a detailed x-ray powder diffraction and computational study of α-Mn up to 220 GPa. Surprisingly, no pressure-induced phase transition was experimentally observed up to the highest pressure of this study, and manganese remains in the α-Mn phase. Interestingly, our density functional theory (DFT) calculations predict that the hcp Mn phase becomes lower in enthalpy than the α-Mn phase above 160 GPa, which suggests the hcp phase is energetically favorable at high pressure. The apparent discrepancy is attributed to a significant kinetic energy barrier separating the α-Mn phase from the hcp phase. Substantial electron transfer, as concluded from the result of Bader charge analysis [5], between Mn atoms in the α-Mn phase results in an ioniclike bonding and stabilizes this phase over the purely metallic hcp Mn.

II. METHODS

A. Experimental methods

High-purity commercially available (Sigma-Aldrich, > 99.9%) fine powder of Mn was used for the angle dispersive XRD measurements. The sample was loaded into a diamond anvil cell with neon as a pressure-transmitting medium

*yansun.yao@usask.ca
†stavrou1@llnl.gov, Present address: Materials and Engineering Science Program, Guangdong Technion-Israel Institute of Technology, Shantou, Guangdong, 515063, China and Technion-Israel Institute of Technology, Haifa, 32000, Israel

(PTM). A Pilatus 1M CdTe detector was used at the undulator XRD beamline at GeoSoilEnviroCARS (sector13), Advanced Photon Source (APS), Chicago, to collect pressure-dependent x-ray diffraction data. The x-ray probing beam spot size was focused to approximately 2–4 μm; additional details on the XRD experimental setups are given in Ref. [6]. Pressure was determined using a known room temperature equation of state (EOS) of Ne [7]. Integration of powder diffraction patterns to yield scattering intensity versus 2θ diagrams and initial analysis were performed using the DIOPTAS program [8]. Calculated XRD patterns were produced using the POWDER CELL program [9] for the corresponding crystal structures according to the EOSs determined experimentally and theoretically in this study and assuming continuous Debye rings of uniform intensity. Le Bail refinements were performed using the GSAS software [10]. Indexing of XRD patterns was performed using the DICVOL program [11] as implemented in the FULLPROF SUITE.

B. Theoretical methods

First-principles calculations were performed using the spin-polarized version of the Vienna Ab initio Simulation Package (VASP) [12]. The generalized gradient approximation was employed with projected augmented wave potentials [13,14] and the Perdew-Burke-Ernzerhof exchange correlation functional [15]. The wave functions were expanded in a plane wave basis set with an energy cutoff of 300 eV. The valence electron configuration of $3p^6 3d^5 4s^2$ for the Mn atom was employed. A crystal structure search was carried out using the particle swarm-intelligence optimization algorithm [16,17]. All predicted crystal structures were processed through density functional theory calculations. Since we are interested in the high-pressure (simple) phases of Mn, a structure search was carried out at 100, 165, and 230 GPa with unit cells containing between 2 and 20 Mn atoms. Lattice dynamical calculations were performed using the linear response Hessian matrix obtained using the VASP program on a $7 \times 7 \times 7$ q-point mesh and a $2\pi \times 0.08$ Å^{-1} k-point spacing and postprocessed using the PHONOPY code [18].

C. Results and discussion

Figure 1 shows integrated diffraction patterns of Mn at selected pressures up to 220 GPa. No discontinuous changes (e.g., appearance of new Bragg peaks) are observed, and all the main Bragg peaks of the α-Mn phase are observed up to the highest pressure of this study. Moreover, no sign of the Bragg peak attributed to bcc Mn by Fujihisa and Takemura (expected at 10.9° in the pattern in the inset of Fig. 1) is observed in any of the patterns in our study, and all observed Brag peaks can be indexed with the α-Mn phase.

From the XRD data, the cell volume of the α-Mn structure is determined as a function of pressure and compared with the values reported in Ref. [2] (see Fig. 2). Our obtained EOS implies a less compressible structure than the one in Ref. [2]. We conducted unweighted fits to the experimental P-V data using a third-order Birch-Murnaghan EOS [19] and determined the bulk modulus B and its first derivative B' at zero pressure: $B_0 = 204(3)$ GPa and $B'_0 = 3.7(4)$. B_0 determined

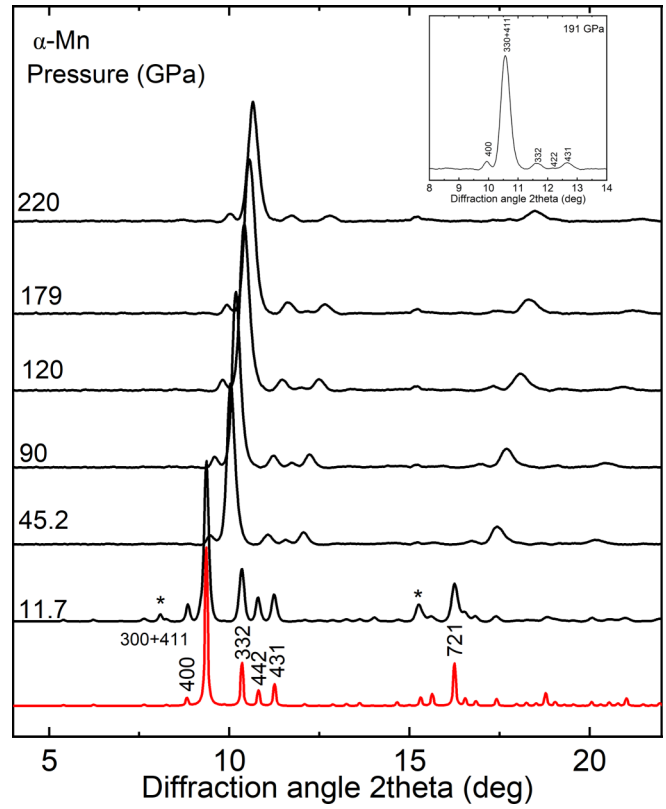

FIG. 1. XRD patterns of α-Mn at selected pressures on pressure increase. The red pattern is the calculated pattern of α-Mn at 14 GPa. Miller indices of the main peaks are also noted. The asterisks mark Bragg peaks from the rhenium gasket. The inset shows an expanded view of the pattern at 191 GPa. The x-ray wavelength is $\lambda = 0.3344$ Å.

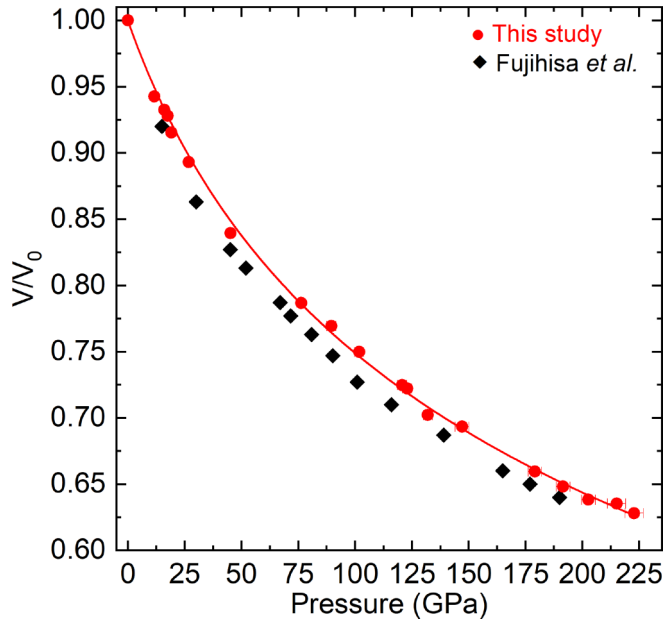

FIG. 2. (a) Volume-pressure data for α-Mn. The solid curve is an unweighted third-order Birch-Murnaghan EOS fit to the experimental data points [19]. The data from Ref. [2] (black dots) are also plotted for comparison.

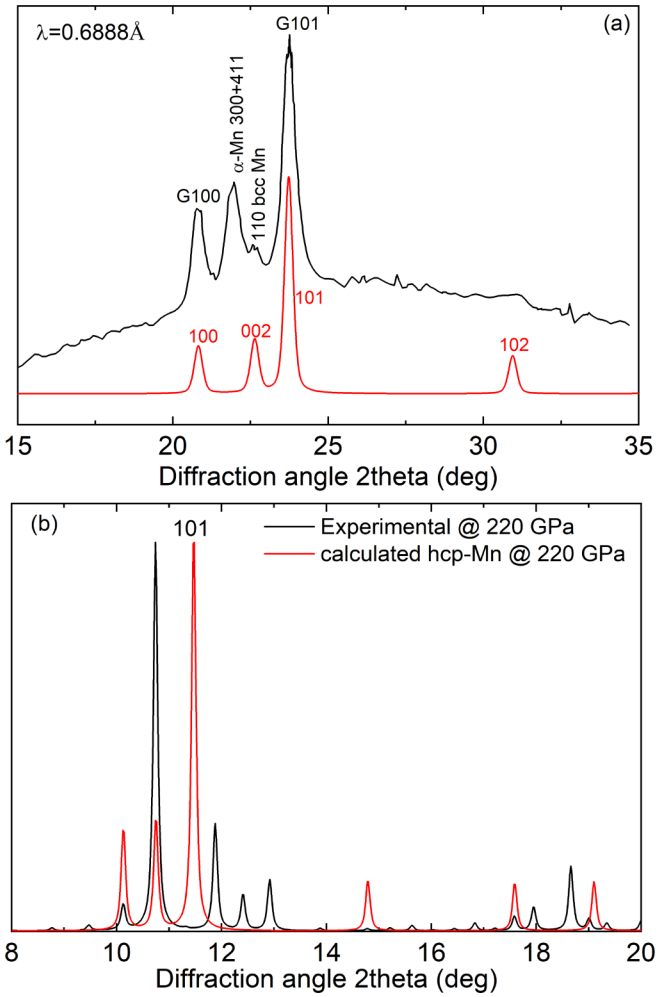

FIG. 3. (a) Comparison between the XRD pattern of Mn at 190 GPa from Ref. [2] (black) and the calculated pattern of hcp Fe at 190 GPa (red) using the EOS of Ref. [23]. Miller indices of hcp Fe are denoted. Miller indices in the experimental pattern are initial indices taken from Ref. [2]. The peaks indexed G100 and G101 are Bragg peaks from the Fe gasket. (b) Comparison between the experimental XRD patten of this study (black) and the calculated pattern of hcp Mn using the calculated EOS of this study (red).

in this study is substantially higher, while B_0' is lower than the ones determined by Fujihisa and Takemura using the Vinet EOS [20]: $B_0 = 158(3)$ GPa and $B_0' = 4.6$. Using a fixed $B_0' = 4.6$ and Vinet EOS, we determined $B_0 = 176(1)$ GPa, which is closer to the value in Ref. [2]. One possible explanation for the difference in the determined elastic parameters might be the different methods used in the two studies for pressure determination: Ne EOS in our study [7] and Fe (gasket) EOS in Ref. [2]. Use of the gasket as a pressure marker could provide an inaccurate pressure [21,22]. We do not expect that the use of Ne as the PTM in our study as opposed to a 4:1 mixture of methanol and ethanol in Ref. [2] should play a role at these pressures [23].

Aiming to resolve the discrepancy concerning the presence of the additional Bragg peak in the study of Fujihisa and Takemura, in Fig. 3(a) we compare the experimental XRD pattern of Mn at 190 GPa from Ref. [2] and the calculated

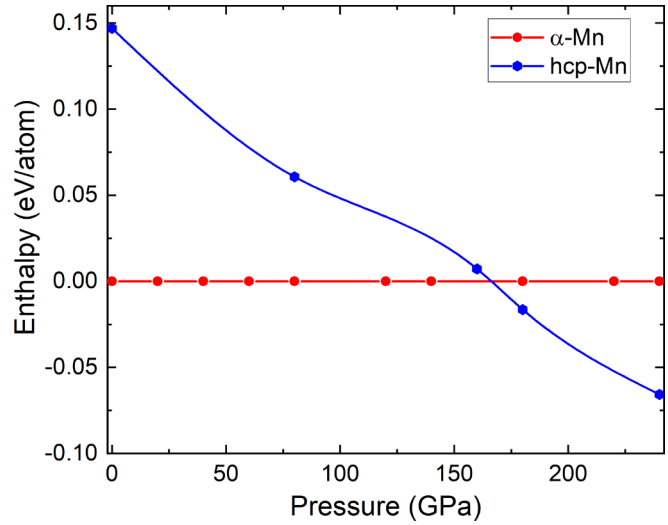

FIG. 4. Calculated enthalpy differences for α-Mn and hcp Mn phases as a function of pressure. The enthalpy of the α-Mn phase is taken as the reference.

pattern of hcp Fe at 190 GPa using the EOS of Ref. [23]. As can clearly be seen, the new Bragg peak initially attributed to the 110 peak of bcc Mn in Ref. [2] can be indexed with the 002 peak of hcp Fe (gasket) in addition to the other peaks already index with the 100 and 101 reflections of Fe. Moreover, in the patterns of Ref. [2] the relative intensity of the new peak appears to follow the same relative intensity increase as the other two Bragg peaks of hcp Fe with increasing pressure. Based on these two observations, it is plausible to conclude that the Bragg peak observed above 160 GPa in Ref. [2] is actually an additional (002) peak originating from the gasket and, in reality, there is no pressure-induced phase transition of Mn taking place, in agreement with our study.

The intuitive expectation on elemental metals under pressure is that they are all likely to favor close-packed structures (hcp, fcc, and variants). At sufficient compression, when most valence electrons are pushed into interstitial sites, the crystal structure of elemental metals is mainly determined by the packing of the cations, similar to the situation at ambient conditions, and therefore, close-packed structure would emerge. To investigate this possibility, we carried out a crystal structure search at 100, 165, and 230 GPa, which bracket the transition pressure reported by Fujihisa and Takemura [2] and the maximum pressure reached in this study. The hcp Mn (space group $P6_3/mmc$) was found to be the most energetically favorable phase, followed by fcc Mn (space group $Fm\text{-}3m$), and bcc Mn (space group $Im\text{-}3m$) was the least stable. This finding is consistent with the results of Zheng-Johansson *et al.* [3], where the hcp phase was reported as the most stable one compared with the bcc and fcc structures. Specifically, the calculated relative enthalpies of α-Mn and hcp Mn as a function of pressure (Fig. 4) show that the hcp phase becomes lower in enthalpy than α-Mn above 165 GPa, implying a possible phase transition above this pressure. For this reason in Fig. 3(b) we compare the experimental pattern of this study with the calculated pattern of hcp Mn using the EOS of hcp Mn calculated in this study. Obviously, there is

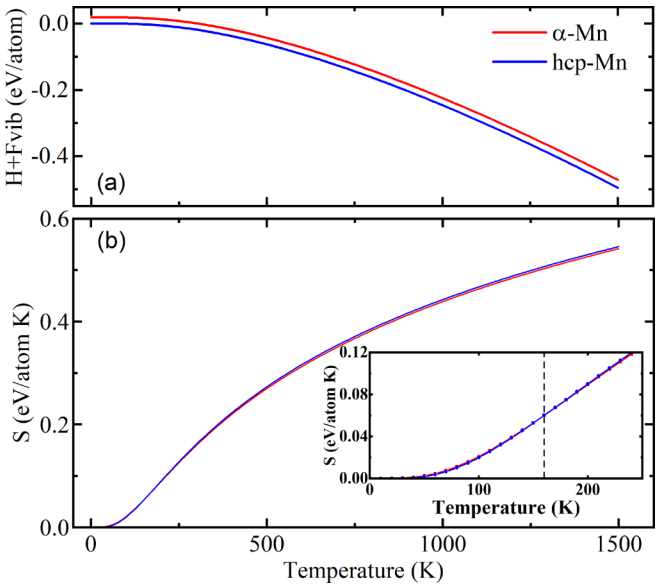

FIG. 5. The temperature-dependent (a) $H + F_{vib}$ for α-Mn and hcp Mn at 180 GPa (see text). The enthalpy of hcp Mn at 0 K was used as the zero-point reference. (b) Vibrational entropies of α-Mn and hcp Mn at 180 GPa. The inset shows hcp Mn having slightly lower vibrational entropies below 160 K.

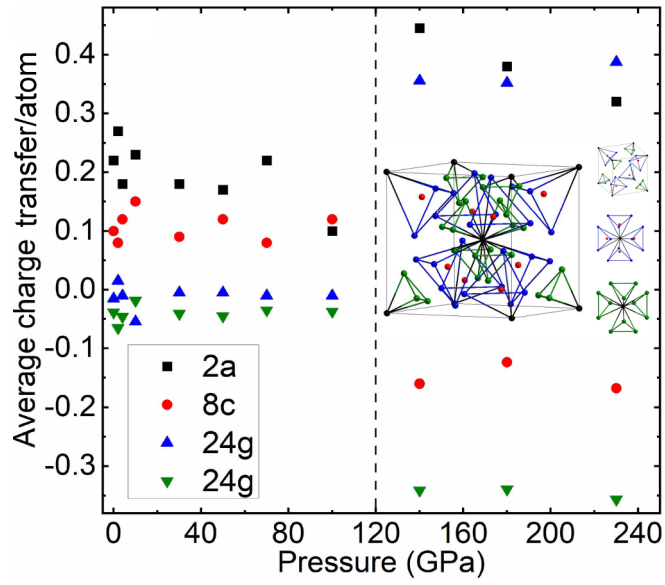

FIG. 6. Average per atom Bader charge transfer of Mn ions in the corresponding Wyckoff positions as a function of pressure, as calculated in this study.

a strong discrepancy between the two patterns, thus ruling out the presence of hcp Mn, even at the level of coexistence with α-Mn (the strongest 101 peak of hcp Mn cannot be observed).

Below the melting point of a material, the lattice contribution to the free energy F_{vib} can play an important role in the relative stability of two different phases [24,25]. We therefore analyze the effects of lattice vibration on both α-Mn and hcp Mn at a pressure (180 GPa) that is slightly above the calculated α-Mn $\rightarrow$ hcp Mn transition. The calculated $H + F_{vib}$ for α-Mn and hcp Mn at 180 GPa are shown in Fig. 5(a) as functions of temperature. The enthalpies H are taken from the static calculation (Fig. 4). The hcp Mn is generally more stable than α-Mn up to the maximum temperature (1500 K), indicating the absence of any lattice dynamic or thermally induced phase transition.

The calculated temperature dependence of the vibrational entropies S of the two phases are shown in Fig. 5(b). Below 160 K, the entropy of α-Mn is slightly higher than that of hcp Mn. Although, in this temperature range, the entropic contribution to the free-energy difference is finite and in favor of α-Mn [see Fig. 5(b), inset], it is much less than the internal energy difference and therefore cannot induce a phase transition from hcp Mn to α-Mn. In fact, at 0 K, hcp Mn is 0.020 eV/atom more stable than α-Mn. In the same vein, at sufficiently high temperature (above 160 K) below the melting temperature of Mn, hcp Mn has a slightly higher entropy and is progressively more stable than the α-Mn, e.g., 0.023 eV/atom more stable than α-Mn at 1500 K. Thus, in the pressure range of interest, the lack of transition to hcp Mn is not likely due to temperature effects.

To gain further insight into the extended pressure stability of the α-Mn phase and, more importantly, to understand the discrepancy between experimental and theoretical results we examined alternative mechanisms that can stabilize the α-Mn phase. In this context, we performed charge transfer calculations in both the α-Mn and hcp Mn phases as a function of pressure using Bader analysis [5]. In the case of hcp Mn, no charge transfer between Mn ions was observed for the whole pressure range of this study. On the other hand, a surprisingly substantial charge transfer is predicted for Mn ions in the α-Mn phase above 100 GPa for all four crystallographically inequivalent Wyckoff positions (2a, 8c, 24g, and 24g). As can clearly be seen in Fig. 6, the charge transfer is low up to 100 GPa, followed by a first-order-like increase above this pressure.

This effect can be described as a pressure-induced autoionization of the Mn atoms, forming a self-salt, in the α-Mn phase. The α-Mn structure is arranged in a cubic unit cell with 2a atoms occupying the corners and center of the cube. The first set of 24g atoms is split into eight three-atom groups, which form four tetrahedrons with four cornered 2a atoms and a cluster of four tetrahedrons sharing one vertex made of the centered 2a atom. The 8c atoms occupy the voids of eight tetrahedrons, forming nominal eight [Mn_5] entities. These filled tetrahedrons have large Mn-Mn contacts, ranging between 3.5 and 3.9Å (ambient value). The second set of 24g atoms also split into eight three-atom groups and form empty tetrahedrons with the 2a atoms exactly the same way. The empty tetrahedrons have smaller size (Mn-Mn distance: 2.1–2.4 Å), nominally [Mn_4] entities. Another way of explaining the structure is that in the bcc unit cell each of the eight cornered Mn atoms forms a tetrahedron with three Mn atoms, and the centered Mn atom forms a cluster of eight tetrahedrons with 24 Mn atoms sharing the center vertex. The unit cell therefore contains 16 tetrahedrons, but only 8 are filled by 8c atoms, resulting in alternating small (empty) and large (filled)

three-dimensional extension of tetrahedrons (see the inset in Fig. 6).

The calculated Bader charges (Fig. 6) reveal substantial charge transfer from the small tetrahedrons to large tetrahedrons nearby, forming self-ionized $[Mn_4]^{\delta+}$ and $[Mn_5]^{\delta-}$ pairs. Interestingly, the abrupt increase of the charge transfer happens slightly below the pressure (165 GPa) at which hcp Mn becomes lower in enthalpy than the α-Mn phase. Thus, it is plausible to conclude that the ionic (in addition to the metallic) character of the bonding in the α-Mn phase above 120 GPa, as opposed to the purely metallic bonding in the hcp Mn phase, is the driving reason for the stability of the α-Mn phase.

The occurrence of such strong charge transfer in an elemental solid is rare. An early theoretical study suggested that solid hydrogen can polarize into H^+H molecules under pressure [26]. Subsequently, autoionization was observed in a few elemental solids at high pressure, such as in the case of the insulating $hP4$ phase of Na [27], γ-phase of B [28], and the predicted N_6 allotrope [29] and the all-nitrogen metallic salt [30]. In these cases ionic bonding involves either localized electrons (electride phases of alkali metals) or molecularlike (e.g., $N_2^{\delta+}$ and $N_5^{\delta-}$) entities. In general, ionicity in elemental solids is the result of many-body interactions, which are stronger in squeezed volumes when orbital splitting is enhanced. The α-Mn structure is made of two tetrahedrons with very different electronic structures. Under high pressure, the filled $[Mn_5]$ tetrahedron becomes anionic and more stable because its neutral state would have an unoccupied bonding orbital. This orbital creates an acceptor band below the Fermi level that receives the electrons transferred from the $[Mn_4]$ tetrahedron nearby. After this, substantial nearest-neighbor electrostatic attraction arises between $[Mn_4]^{\delta+}$ and $[Mn_5]^{\delta-}$, resulting in a very high cohesive energy making the α-Mn phase metastable in an extended pressure range.

Another interesting point to note is that from the crystallographic point of view, the α-Mn and hcp Mn phases are not linked by either a group-subgroup relation or a common subgroup. This means that the α-Mn $\rightarrow$ hcp Mn phase transition, if it ever happens, will likely proceed in an abrupt manner with no clearly defined order parameters [31]. Such a transition is associated with a very high activation barrier compared to a displacive reconstructive phase transition. However, since the phase transition path cannot be uniquely described (by collective variables), we cannot estimate the energy barrier for the α-Mn $\rightarrow$ hcp Mn transition. This kind of dynamic stability is commonplace for materials under high pressure, where interesting crystal structures/stoichiometries were found to be stable beyond their pressure range of stability [32]. From the above discussion it is plausible to conclude that the extended stability of the α-Mn could be attributed to both the ionic character of this phase above 120 GPa and also the presumably high energy barrier.

D. Conclusion

Our study calls for follow-up experimental (e.g., an x-ray appearance near-edge structure might provide experimental evidence of the charge transfer, although the critical pressure is relatively high for such measurements [33]) and theoretical studies aiming to fully elucidate the mechanism of the stability of the α-Mn phase. Our Bader analysis revealed that under pressure, in addition to electride phases and molecularlike salts, ionic bonding in elemental solids could also exist between exclusively monatomic ions of the same metallic element.

ACKNOWLEDGMENTS

This work was performed under the auspices of the U.S. Department of Energy by Lawrence Livermore National Security, LLC, under Contract No. DE-AC52-07NA27344. This work was supported by DARPA (Grants No. W31P4Q1310005 and No. W31P4Q1210008), the Deep Carbon Observatory, and the Natural Sciences and Engineering Research Council of Canada. This research used resources of the Advanced Photon Source, a U.S. Department of Energy (DOE) Office of Science User Facility operated for the DOE Office of Science by Argonne National Laboratory under Contract No. DE-AC0206CH11357. GSECARS is supported by the U.S. NSF (Grant No. EAR-1128799) and DOE Geosciences (Grant No. DE-FG02-94ER14466). Use of the COMPRES-GSECARS gas loading system was supported by COMPRES under NSF Cooperative Agreement No. EAR -1606856 and by GSECARS through NSF Grant No. EAR-1634415 and DOE Grant No. DE-FG02-94ER14466. The authors thank S. N. Tkachev for help with gas loading samples at the APS, Sector-13 GSECARS beamline. E.S. thanks K. Syassen for fruitful discussions and for a critical reading of the manuscript. E.S. was partially supported by LDRD Grant No. 18-LW-036.

[1] L. Brewer, Science **161**, 115 (1968).
[2] H. Fujihisa and K. Takemura, Phys. Rev. B **52**, 13257 (1995).
[3] J. X. Zheng-Johansson, O. Eriksson, B. Johansson, L. Fast, and R. Ahuja, Phys. Rev. B **57**, 10989 (1998).
[4] K. Takemura, O. Shimomura, K. Hase, and T. Kikegawa, J. Phys. F **18**, 197 (1988).
[5] R. F. W. Bader, *Atoms in Molecules: A Quantum Theory* (Oxford University Press, Oxford, 1990).
[6] V. B. Prakapenka, A. Kubo, A. Kuznetsov, A. Laskin, O. Shkurikhin, P. Dera, M. L. Rivers, and S. R. Sutton, High Pressure Res. **28**, 225 (2008).
[7] A. Dewaele, F. Datchi, P. Loubeyre, and M. Mezouar, Phys. Rev. B **77**, 094106 (2008).
[8] C. Prescher and V. B. Prakapenka, High Pressure Res. **35**, 223 (2015).
[9] W. Kraus and G. Nolze, J. Appl. Crystallogr. **29**, 301 (1996).

[10] A. C. Larson and R. B. V. Dreele, Los Alamos National Laboratory, Technical Report No. LAUR 86-748, 2000 (unpublished).
[11] A. Boultif and D. Louër, J. Appl. Crystallogr. **37**, 724 (2004).
[12] G. Kresse and J. Furthmüller, Comput. Mater. Sci. **6**, 15 (1996).
[13] G. Kresse and D. Joubert, Phys. Rev. B **59**, 1758 (1999).
[14] P. E. Blöchl, Phys. Rev. B **50**, 17953 (1994).
[15] J. P. Perdew, K. Burke, and M. Ernzerhof, Phys. Rev. Lett. **77**, 3865 (1996).
[16] Y. Wang, J. Lv, L. Zhu, and Y. Ma, Phys. Rev. B **82**, 094116 (2010).
[17] Y. Wang, J. Lv, L. Zhu, and Y. Ma, Comput. Phys. Commun. **183**, 2063 (2012).
[18] A. Togo, F. Oba, and I. Tanaka, Phys. Rev. B **78**, 134106 (2008).
[19] F. Birch, J. Geophys. Res. **83**, 1257 (1978).
[20] P. Vinet, J. R. Smith, J. Ferrante, and J. H. Rose, Phys. Rev. B **35**, 1945 (1987).
[21] S. Anzellini, A. Dewaele, F. Occelli, P. Loubeyre, and M. Mezouar, J. Appl. Phys. **115**, 043511 (2014).
[22] A. Dewaele and P. Loubeyre, High Pressure Res. **27**, 419 (2007).
[23] A. Dewaele, P. Loubeyre, F. Occelli, M. Mezouar, P. I. Dorogokupets, and M. Torrent, Phys. Rev. Lett. **97**, 215504 (2006).
[24] P. Pavone, S. Baroni, and S. de Gironcoli, Phys. Rev. B **57**, 10421 (1998).
[25] A. A. Adeleke, M. J. Greschner, A. Majumdar, B. Wan, H. Liu, Z. Li, H. Gou, and Y. Yao, Phys. Rev. B **96**, 224104 (2017).
[26] B. Edwards and N. W. Ashcroft, Nature (London) **388**, 652 (1997).
[27] Y. Ma, M. Eremets, A. R. Oganov, Y. Xie, I. Trojan, S. Medvedev, A. O. Lyakhov, M. Valle, and V. Prakapenka, Nature (London) **458**, 182 (2009).
[28] A. R. Oganov, J. Chen, C. Gatti, Y. Ma, Y. Ma, C. W. Glass, Z. Liu, T. Yu, O. O. Kurakevych, and V. L. Solozhenko, Nature (London) **457**, 863 (2009).
[29] M. J. Greschner, M. Zhang, A. Majumdar, H. Liu, F. Peng, J. S. Tse, and Y. Yao, J. Phys. Chem. A **120**, 2920 (2016).
[30] J. Sun, M. Martinez-Canales, D. D. Klug, C. J. Pickard, and R. J. Needs, Phys. Rev. Lett. **111**, 175502 (2013).
[31] H. T. Stokes and D. M. Hatch, Phys. Rev. B **65**, 144114 (2002).
[32] A. O. Adeniyi, M. Kunz, E. Stavrou, and Y. Yao, Phys. Rev. Res. **2**, 033072 (2020).
[33] D. Levy, E. Greenberg, S. Layek, M. P. Pasternak, I. Kantor, S. Pascarelli, C. Marini, Z. Konopkova, and G. K. Rozenberg, Phys. Rev. B **101**, 245121 (2020).